Inelastic neutrino scattering off hot nuclei in supernova environments

Alan A. Dzhioev,[1,*] A. I. Vdovin,[1] J. Wambach,[2,3] and V. Yu. Ponomarev[2]

[1] *Bogoliubov Laboratory of Theoretical Physics, JINR, 141980, Dubna, Russia*
[2] *Institut für Kernphysik, Technische Universität Darmstadt, 64289 Darmstadt, Germany*
[3] *GSI Helmholtzzentrum für Schwerionenforschung, Planckstr. 1, 64291 Darmstadt, Germany*

(Dated: January 17, 2014)

We study inelastic neutrino scattering off hot nuclei for temperatures relevant under supernova conditions. The method we use is based on the quasiparticle random phase approximation extended to finite temperatures within the thermo field dynamics (TQRPA). The method allows a transparent treatment of upward and downward transitions in hot nuclei, avoiding the application of Brink's hypothesis. For the sample nuclei ^{56}Fe and ^{82}Ge we perform a detailed analysis of thermal effects on the strength distributions of allowed Gamow-Teller (GT) transitions which dominate the scattering process at low neutrino energies. For ^{56}Fe and ^{82}Ge the finite temperature cross-sections are calculated by taking into account the contribution of allowed and forbidden transitions. The observed enhancement of the cross-section at low neutrino energies is explained by considering thermal effects on the GT strength. For ^{56}Fe we compare the calculated cross-sections to those obtained earlier from a hybrid approach that combines large-scale shell-model and RPA calculations.

PACS numbers: 26.50.+x, 21.60.Jz, 24.10.Pa, 25.30.Pt

arXiv:1401.4008v1 [nucl-th] 16 Jan 2014

I. INTRODUCTION

The significant role played by processes involving neutrinos in core-collapse supernovae (type II supernovae) is well known [1]. Until the core reaches densities of $\rho \sim 10^{11}\,\mathrm{g\,cm^{-3}}$, a substantial amount of the gravitational energy of the collapse is radiated by neutrinos that leave the star freely. However, at higher densities neutrino interactions with matter become important on the time-scale of the collapse, leading to neutrino trapping and thermalization. Supernova core-collapse simulations require a detailed description of neutrino transport and should in principle include all potentially important neutrino reactions.

It was first pointed by Haxton [2] that the neutral-current inelastic neutrino scattering on nuclei involving the excitation of giant resonances can lead to significant neutrino cross-sections and, therefore, this process should be incorporated into core-collapse simulations. Shortly thereafter, this was done by Bruenn and Haxton [3]. They found that the inelastic neutrino-scattering on nuclei plays the same important role as the neutrino-electron scattering in equilibrating neutrinos with matter (see also Ref. [4]).

In their study Bruenn and Haxton approximated the nuclear composition of the core by a single representative nucleus, ^{56}Fe. Moreover, the relevant cross-sections were calculated by assuming that only allowed Gamow-Teller and first-forbidden upward transitions from the nuclear ground-state contribute to neutrino scattering. However, supernova matter has a temperature of an order of 1 MeV or higher and the neutrinos scatter off nuclei which are in thermally populated excited states. As was first realized in Ref. [5], upward and downward transitions from nuclear excited states to lower-lying states completely remove the energy threshold for the inelastic neutrino-nucleus scattering in the supernova environment and contribute to a significant enhancement of the cross-section for low-energy neutrinos. Moreover, and this is more important, due to downward transitions from nuclear excited states to lower-lying states neutrinos can gain energy after interacting with the nucleus, thereby assisting in cooling the core and reducing its entropy. This is different to inelastic scattering with electrons where due to the degeneracy of electrons neutrinos mainly loose energy.

An explicit calculation of reaction rates and cross-sections at finite temperature can be performed by summing over Boltzmann-weighted, individually determined contributions from nuclear excited states. However, for $T \gtrsim 1\,\mathrm{MeV}$ a state-by-state evaluation includes too many states to derive the cross section for each individual state and, hence, is unfeasible. To overcome this difficulty an approximate method to treat thermal effects on the inelastic neutrino-nucleus scattering was proposed in [6] (see also Ref. [7]) within the so-called hybrid approach [8, 9]. In this method the contributions of the allowed Gamow-Teller transitions to the neutrino-nucleus cross-section are derived from large-scale shell-model (SM) calculations, while the forbidden contributions are considered within the RPA.

To treat thermal effects within the hybrid approach, the Gamow-Teller contribution to the cross-section is split into the neutrino down-scattering ($E_{\nu'} < E_\nu$) and neutrino up-scattering ($E_{\nu'} > E_\nu$) parts, where E_ν, $E_{\nu'}$ denote the neutrino energies in the initial and final states, respectively. For the down-scattering part the Brink hypothesis was applied which states that GT distributions built on nuclear excited states are the same as those for the nuclear ground state but shifted by the excitation energy. Under this assumption, the down-scattering part of

* dzhioev@theor.jinr.ru

the cross-section becomes temperature independent. The temperature dependence arises from the up-scattering part which accounts for contributions of downward transitions from nuclear excited states. These contributions are determined by 'inversion' of the shell-model GT distributions for the low-lying states.

Large-scale shell-model calculations provide a detailed strength distribution of charge-neutral Gamow-Teller (GT_0) transitions that strongly dominate the inelastic neutrino-nucleus scattering at low neutrino energies ($E_\nu \lesssim 15\,\mathrm{MeV}$). However, being applied to hot nuclei, this method has its own shortcomings mainly because it partially employs the Brink hypothesis when treating GT_0 transitions from nuclear excited states. As follows from experimental studies of giant dipole resonances (GDR) in hot nuclei, the GDR strength function exhibits a temperature dependence (see, e.g., the monograph [10] and one of the latest reviews [11]), i.e., the validity of the Brink hypothesis is not obvious. Moreover, theoretical calculations performed for charge-exchange GT transitions in the framework of the shell-model Monte Carlo (SMMC) method demonstrate that with increasing temperature the GT centroid shifts to lower energies and the width of the distribution increases with the appearance of low-lying states [12]. In addition, the present computer capabilities allow application of large-scale shell-model calculations only to iron group nuclei (pf-shell, $A = 45 - 65$), whereas neutrino scattering on more massive and neutron-rich nuclei also may play an important role in various astrophysical scenarios. Thus, the problem of an accurate description of inelastic neutrino-nucleus scattering in the supernova environment is not solved completely yet and alternative methods are desirable.

In [13], we have developed such an alternative approach to treat thermal effects on inelastic neutrino-nucleus scattering cross-sections. This approach is based on the thermal quasiparticle random phase approximation (TQRPA). We apply it in the context of the thermo field dynamics (TFD) formalism [14–16] which enables a transparent treatment of upward and downward transitions from thermally excited nuclear states and opens possibilities for systematic improvements. This approach was also recently used in studies of the electron capture on hot nuclei under supernova conditions [17].

In [13], the thermal effects on the inelastic neutrino scattering off the hot ^{54}Fe nucleus were investigated. It was shown that the TQRPA does not support Brink's hypothesis and leads to temperature dependent strength distributions for allowed and forbidden transitions. As a result, both the up- and down-scattering parts of the cross-section are temperature dependent. Despite the differences between the two approaches, the TQRPA revealed the same thermal effect as was found in [6]. Namely, a temperature increase results in considerable enhancement of the cross-section for neutrino energies lower than the energy of the GT_0 resonance.

In the present paper, we extend our previous study by also considering inelastic neutrino scattering off neutron-rich nuclei beyond pf-shell. In our calculations, we take into account not only the first-forbidden transitions but also contributions from higher multipoles. For the selected iron isotope, ^{56}Fe, we perform a detailed comparison of the calculated TQRPA cross-sections with the hybrid approach results and discuss the reason for the observed discrepancy at low neutrino energies.

The paper is organized as follows. In Sec. II we present some important features of the TFD formalism and briefly outline how to treat upward and downward transitions in a hot nucleus within the TQRPA. The details of our approach are expounded in [13, 17, 18]. In Sec. II, we also provide the necessary formulas to calculate inelastic neutrino-nucleus cross-sections at finite temperatures. The results of the numerical calculations are presented and discussed in Sec. III for the sample nuclei ^{56}Fe and ^{82}Ge. The conclusions are summarized in Sec. IV.

II. FORMALISM

In the stellar environment during the core-collapse phase all nuclear reactions mediated by the strong and electromagnetic interaction are in equilibrium with their inverse [1]. Neglecting weak-interaction mediated reactions, nuclei are in thermal equilibrium with heat and particle reservoirs and, therefore, can be described as a thermal ensemble. In TFD, such an equilibrium ensemble is represented by a temperature-dependent state termed the thermal vacuum $|0(T)\rangle$ [19]. The thermal vacuum is determined as the zero-energy eigenstate of the thermal Hamiltonian, $\mathcal{H} = H - \widetilde{H}$, and it satisfies the thermal state condition

$$A|0(T)\rangle = \sigma_A \mathrm{e}^{\mathcal{H}/2T} \widetilde{A}^\dagger |0(T)\rangle. \tag{1}$$

In the above equations H is the original nuclear Hamiltonian and $\widetilde{H}$ is its tilde counterpart acting in the auxiliary Hilbert space; an operator A acts in the physical Hilbert space, $\widetilde{A}$ is its tilde partner, and σ_A is a phase factor. The thermal state condition guarantees that the expectation value $\langle 0(T)|A|0(T)\rangle$ is equal to the (grand)canonical average of A. In this sense, relation (1) is equivalent to the Kubo-Martin-Schwinger condition for an equilibrium (grand)canonical density matrix [20].

Weak-interaction processes, such as inelastic neutrino scattering, induce transitions from the thermal vacuum to excited states of the thermal nuclear Hamiltonian. As follows from the definition of $\mathcal{H}$, each of its eigenstates with positive energy has a counterpart — the tilde-conjugate eigenstate — with negative but same absolute value of energy. Transitions from the thermal vacuum to positive energy states (upward transitions) correspond to excitation of the nucleus, while transitions to negative energy states (downward transitions) describe the decay of thermally excited states.

A. Thermal quasiparticle RPA

Let us now consider a general nuclear Hamiltonian consisting of mean fields for protons and neutrons, pairing interactions, and residual two-nucleon interactions:

$$H = H_{\rm mf} + H_{\rm pair} + H_{\rm res}. \quad (2)$$

To fix an average number of protons and neutrons we introduce the respective chemical potentials into $H_{\rm mf}$. The residual interaction can contain both particle-hole and particle-particle terms. We assume a spherically symmetric nucleus, although the deformation can be easily included into the theory. Within the TQRPA, to find excited states of a hot nucleus, we first introduce thermal quasiparticle creation ($\beta^\dagger$, $\widetilde{\beta}^\dagger$) and annihilation ($\beta$, $\widetilde{\beta}$) operators which account for pairing correlations at finite temperature. The structure of this operators is found by diagonalizing the $\mathcal{H}_{\rm mf}+\mathcal{H}_{\rm pair}$ part of the thermal Hamiltonian and simultaneously demanding that the vacuum of thermal quasiparticles obeys the thermal state condition (1). Then, to account for the long-range residual interaction, we introduce thermal phonon operators $Q^\dagger_{JMi}$, $\widetilde{Q}^\dagger_{JMi}$ of given total angular momentum (J, M) whose action on the thermal vacuum $|0(T)\rangle$ creates thermal excited states, while the thermal vacuum itself is the vacuum for the Q_{JMi}, $\widetilde{Q}_{JMi}$ operators.

The structure and the energy of thermal phonons can be found by applying either the variational principle or the equation of motion method under two additional constraints: (i) phonon operators commute like bosonic ones; (ii) the vacuum of thermal phonons obeys the thermal state condition (1). The resulting phonon operators have the following form [21]:

$$Q^\dagger_{JMi} = \sum_{j_1 j_2}\Big\{\psi^{Ji}_{j_1 j_2}[\beta^\dagger_{j_1}\beta^\dagger_{j_2}]^J_M + \widetilde{\psi}^{Ji}_{j_1 j_2}[\widetilde{\beta}^\dagger_{\overline{j_1}}\widetilde{\beta}^\dagger_{\overline{j_2}}]^J_M + \eta^{Ji}_{j_1 j_2}[\beta^\dagger_{j_1}\widetilde{\beta}^\dagger_{\overline{j_2}}]^J_M + \phi^{Ji}_{j_1 j_2}[\beta_{\overline{j_1}}\beta_{\overline{j_2}}]^J_M + \widetilde{\phi}^{Ji}_{j_1 j_2}[\widetilde{\beta}_{j_1}\widetilde{\beta}_{j_2}]^J_M + \xi^{Ji}_{j_1 j_2}[\beta_{\overline{j_1}}\widetilde{\beta}_{j_2}]^J_M\Big\} \quad (3)$$

and they diagonalize the thermal Hamiltonian

$$\mathcal{H} \simeq \sum_{JMi}\omega_{Ji}(T)(Q^\dagger_{JMi}Q_{JMi} - \widetilde{Q}^\dagger_{JMi}\widetilde{Q}_{JMi}) \quad (4)$$

within the TQRPA. The phonon amplitudes ψ, $\widetilde{\psi}$, etc. as well as the phonon energies ω are the solution of the TQRPA equations. It should be emphasized that in the zero-temperature limit the TQRPA method turns into the standard QRPA.

In [17], we have performed a detailed analysis of finite temperature effects on the spectrum of charge-exchange thermal phonons. Here we repeat the main conclusions which remain valid for the charge-neutral excitations as well. Due to the terms in (3) involving tilde thermal quasiparticle operators (terms like $\beta^\dagger\widetilde{\beta}^\dagger$ and $\widetilde{\beta}^\dagger\widetilde{\beta}^\dagger$) the spectrum of thermal phonons contains negative- and low-energy states which do not exist at zero temperature. Since (see [17] for more details) the creation of a tilde quasiparticle is equivalent to the annihilation of a thermally excited Bogoliubov quasiparticle, the excitation of the aforementioned "new" phonon states can be interpreted as thermally unblocked transitions from nuclear excited states. Furthermore, both the energies of thermal quasiparticles and the interaction strength between them are temperature dependent. As a result, after solving the TQRPA equations we obtain a temperature-dependent spectrum of thermal phonons.

Once the structure of thermal phonons is determined, one can evaluate transition strengths (probabilities) from the thermal vacuum to thermal one-phonon states. For a given transition operator $\mathcal{T}$ we have

$$\Phi_{Ji} = \big|\langle Q_{Ji}\|\mathcal{T}\|0(T)\rangle\big|^2,$$
$$\widetilde{\Phi}_{Ji} = \big|\langle \widetilde{Q}_{Ji}\|\mathcal{T}\|0(T)\rangle\big|^2, \quad (5)$$

where Φ_{Ji} and $\widetilde{\Phi}_{Ji}$ are the strengths of upward and downward transitions, respectively. They are connected by the relationship

$$\widetilde{\Phi}_{Ji} = \exp\Big(-\frac{\omega_{Ji}}{T}\Big)\Phi_{Ji}, \quad (6)$$

where ω_{Ji} is a positive solution of the TQRPA equations. This relation links the probabilities to transfer and gain energy $E = \omega_{Ji}$ from a hot nucleus. It is interesting to note that the same relationship between the upward and downward transition strengths is used in [22] when considering the thermal strength functions for emission and absorption of neutrino-antineutrino pairs by hot nuclei. In [22], the relation results from the principle of detailed balance. In TFD, it arises from the thermal state condition imposed on the thermal vacuum. We also would like to point out that in [22], due to the application of Brink's hypothesis, the absorption (upward) strength is considered to be temperature independent and only the emission (downward) strength depends on temperature due to the Boltzmann factor $\exp(-E/T)$. In contrast, within the present approach, both the upward and downward transition strengths are temperature dependent.

B. Cross-section at finite temperatures

Deriving the inelastic neutrino-nucleus cross-section at finite temperature we follow the Walecka-Donnelly formalism [23, 24] which is based on the standard current-current form of the weak interaction Hamiltonian. Then the temperature-dependent differential cross-section for a transition from the thermal vacuum to the final thermal one-phonon state takes the form

$$\frac{d}{d\Omega}\sigma_{Ji}(E_\nu, T) = \frac{2G_F^2}{\pi}\,E_{\nu'}^2\cos^2\frac{\Theta}{2}\big\{\sigma^J_{CL} + \sigma^J_T\big\}. \quad (7)$$

Here, G_F is the Fermi constant of the weak interaction and Θ the scattering angle. The Coulomb-longitudinal, σ^J_{CL}, and transverse, σ^J_T, terms in Eq. (7) are given by

$$\sigma^J_{CL} = |\langle Ji\|\hat{M}_J \pm \frac{\omega_{Ji}}{q}\hat{L}_J\|0(T)\rangle|^2, \tag{8}$$

$$\sigma^J_T = \Big(-\frac{q^2_\mu}{2q^2} + \tan^2\frac{\Theta}{2}\Big)\Big[|\langle Ji\|\hat{T}^{\rm mag}_J\|0(T)\rangle|^2 + |\langle Ji\|\hat{T}^{\rm el}_J\|0(T)\rangle|^2\Big] - \tan\frac{\Theta}{2}\sqrt{-\frac{q^2_\mu}{2q^2} + \tan^2\frac{\Theta}{2}} \times \Big[2{\rm Re}\langle Ji\|\hat{T}^{\rm mag}_J\|0(T)\rangle\langle Ji\|\hat{T}^{\rm el}_J\|0(T)\rangle^*\Big], \tag{9}$$

where $q_\mu = (\pm\omega_{Ji}, \vec{q})$ ($q = |\vec{q}| = \sqrt{\omega^2_{Ji} + 4E_{\nu'}E_\nu\sin^2\frac{\Theta}{2}}$) is the 4-momentum transfer and the notation $|Ji\rangle$ is used to denote both the non-tilde and the tilde states. The upper sign in the above equations refers to upward transitions from the thermal vacuum to non-tilde states ($E_{\nu'} = E_\nu - \omega_{Ji}$), while the lower sign corresponds to downward transitions to tilde states ($E_{\nu'} = E_\nu + \omega_{Ji}$). The multipole operators $\hat{M}_J$, $\hat{L}_J$, $\hat{J}^{\rm el}_J$, and $\hat{J}^{\rm mag}_J$ denote the charge, longitudinal, and transverse electric and magnetic parts of the hadronic current, respectively, as defined in [23, 24]. For the vector, axial-vector, and pseudoscalar form-factors which describe the internal structure of the nucleon we use parametrization from Ref. [25] (see also Ref. [26]).

From Eq. (7), the total cross-section, $\sigma(E_\nu, T)$, as a function of temperature and incoming neutrino energy is obtained by integrating over the scattering angle and summing over all possible final thermal excited states

$$\sigma(E_\nu, T) = 2\pi\sum_{Ji}\int_1^{-1}\frac{d\sigma_{Ji}}{d\Omega}\,d\cos\Theta = \sigma_{\rm down}(E_\nu, T) + \sigma_{\rm up}(E_\nu, T). \tag{10}$$

Here, we follow Ref. [6] and split the total cross-section into two parts: $\sigma_{\rm down}(E_\nu, T)$ describes the neutrino down-scattering process and includes only transitions to non-tilde phonon states, while $\sigma_{\rm up}(E_\nu, T)$ corresponds to the neutrino up-scattering associated with transitions to tilde states.

For inelastic scattering of low-energy neutrinos, i.e., in the long wavelength limit ($q \to 0$), only two multipole operators survive, $\hat{L}_1$ and $\hat{T}^{\rm el}_1$, which contribute to 1^+ transitions. Then the integration over the scattering angle in Eq. (10) can be performed analytically and, in view of the detailed balance principle (6), the low-energy cross-section can be written as

$$\sigma(E_\nu, T) = \frac{G^2_F}{\pi}{\sum_i}'(E_\nu - \omega_i)^2\Phi_i + \frac{G^2_F}{\pi}\sum_i(E_\nu + \omega_i)^2\exp\Big(-\frac{\omega_i}{T}\Big)\Phi_i, \tag{11}$$

where Φ_i is the transition strength for the Gamow-Teller operator (see Eq. (13) below). The sum ${\sum_i}'$ in the first, down-scattering, term implies summation over 1^+ non-tilde thermal phonon states with the energy $\omega_i < E_\nu$. Apparently, for vanishing neutrino energies, $E_\nu \approx 0$, only the second, up-scattering, term persists at finite temperatures. We also note that although the Boltzmann factor suppresses the contributions of downward transitions from high-lying thermally excited states, the phase-space factor $(E_\nu + \omega_i)^2$ acts in the opposite direction and favors them.

III. RESULTS AND DISCUSSION

The formalism presented above is employed to study thermal effects on the inelastic neutrino scattering off the two sample nuclei, ^{56}Fe and ^{82}Ge. The iron isotope is among the most abundant nuclei at the early stage of the core-collapse, while the neutron-rich germanium isotope can be considered as the average nucleus at later stages [27].

Let us now specify the nuclear Hamiltonian which will be used in the present study. Like in [13, 17], we apply a phenomenological Hamiltonian containing separable particle-hole residual interactions with isoscalar and isovector parts. We neglect particle-particle interactions except for the BCS pairing forces. This Hamiltonian is usually referred to as the quasiparticle-phonon model (QPM) [28]. For ^{56}Fe and ^{82}Ge, the single-particle energies and wave-functions are derived from an appropriate Woods-Saxon mean-field potential [29]. The depth of the Wood-Saxon potential as well as the pairing strength parameters are fixed in the same manner as in [13, 17]. In the obtained single-particle level schemes ^{56}Fe has two neutron holes in the $1f_{7/2}$ subshell and two protons in the $2p_{3/2}$ subshell, while ^{82}Ge has closed $1g_{9/2}$ neutron and $2p_{3/2}$ proton subshells. It is notable that the sequence of single-particle levels for ^{82}Ge is close to that used in Ref. [27] for the same nucleus in spite of different Woods-Saxon parameterizations. Solving the BCS equations at zero-temperature we get the proton and neutron pairing gaps: $\Delta_{p(n)} = 1.57(1.36)$ MeV for ^{56}Fe and $\Delta_{p(n)} = 1.22(0.0)$ MeV for ^{82}Ge. Thus, the critical temperature $T_{\rm cr} \approx 0.5\Delta(T=0)$ above which the pairing gap collapses, according to the BCS theory (see Refs. [30, 31] for more details), is $T_{\rm cr} \approx 0.8\,$MeV for ^{56}Fe and $T_{\rm cr} \approx 0.6\,$MeV for ^{82}Ge.

In the present study, multipoles up to $J^\pi = 3^\pm$ contributing to the neutrino-scattering cross-section (7) are included in the calculations. To generate the thermal one-phonon excited states, we use both multipole and

spin-multipole components of the residual interaction

$$H^{\rm ph}_{\rm M} = -\frac{1}{2}\sum_{\lambda\mu}\sum_{\substack{\tau=n,p\\ \rho=\pm1}}(\kappa_0^{(\lambda)}+\rho\kappa_1^{(\lambda)})M^\dagger_{\lambda\mu}(\tau)M_{\lambda\mu}(\rho\tau),$$

$$H^{\rm ph}_{\rm SM} = -\frac{1}{2}\sum_{L\lambda\mu}\sum_{\substack{\tau=n,p\\ \rho=\pm1}}(\kappa_0^{(L\lambda)}+\rho\kappa_1^{(L\lambda)})S^\dagger_{L\lambda\mu}(\tau)S_{L\lambda\mu}(\rho\tau). \quad (12)$$

Here $M^\dagger_{\lambda\mu}$ and $S^\dagger_{L\lambda\mu}$ are single-particle multipole and spin-multipole operators [28], and changing the sign of the isotopic index τ means changing $n \leftrightarrow p$. The excitations of natural parity ($\pi = (-1)^J$) are generated by the multipole and spin-multipole $L = \lambda$ interactions (12), while the spin-multipole interactions with $L = \lambda \pm 1$ are responsible for the states of unnatural parity ($\pi = (-1)^{J+1}$). To generate 0^+ excitations, we take into account both the particle-hole residual interaction and the particle-particle interaction stemming from the pairing part of the Hamiltonian. Here we would like to emphasize that the inclusion of the particle-particle residual interaction into the Hamiltonian does not affect the strength distributions and the cross-sections for temperatures above the critical one.

In contrast to [13, 32], in the present study the radial form-factors of multipole and spin-multipole operators in Eq. (12) have the r^λ form. We found that this form of the radial form-factors gives better agreement with results of relativistic self-consistent QRPA calculations [26] when comparing multipole composition of the cross-sections (see the discussion below). The respective isoscalar and isovector strength parameters, $\kappa_{0,1}^{(\lambda)}$ and $\kappa_{0,1}^{(L\lambda)}$, are first roughly estimated following Refs. [33, 34] and then partly refined on the basis of available experimental data. For example, in ^{56}Fe the isovector strength parameters $\kappa_1^{(01)}$ and $\kappa_1^{(21)}$ are slightly readjusted to reproduce the experimental centroid energies of the GT$_-$ and GT$_+$ resonances [35, 36]. We find that the isovector strength parameter $\kappa_1^{(1)}$ estimated according to [34] reproduces the experimental position of the GDR centroid ($\sim$ 18 MeV) in ^{56}Fe [37] quite well. In addition, the isoscalar strength parameters $\kappa_0^{(1)}$ for ^{56}Fe and ^{82}Ge are fitted to exclude the spurious 1^- state due to the center of mass motion of the nucleus.

A. Zero temperature

Before proceeding to thermal effects we consider the inelastic neutrino-nucleus cross-sections at zero temperature and perform a comparison with the available results of other approaches. We note once again that at $T = 0$ our calculations are equivalent to the QRPA. The calculated ground-state cross-sections for ^{56}Fe and ^{82}Ge are shown in Fig. 1 for incoming neutrino energies $E_\nu = 0 - 60$ MeV. As one can see in the figure,

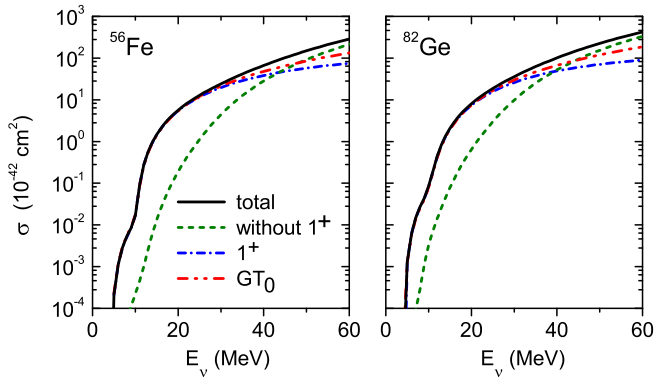

FIG. 1. (Color online) Inelastic neutrino scattering cross-sections off the ground states of ^{56}Fe and ^{82}Ge as functions of the incoming neutrino energy E_ν. The total cross-sections include contributions of $J^\pi = 0^\pm - 3^\pm$ multipoles (solid lines). The dashed lines show the cross-sections calculated when the 1^+ contributions are omitted. The dash-dotted lines display the 1^+ contributions to the cross-sections calculated with the full q-dependent transition operator whereas the 1^+ contributions calculated with the GT$_0$ operator (13) are shown by the dash-double dotted lines.

for neutrinos with $E_\nu < 30$ MeV the total cross-sections are dominated by 1^+ transitions. Due to the energy gap in the 1^+ nuclear states the cross-sections drop rapidly to zero as the neutrino energy approaches the reaction threshold. Within the present QRPA calculations, the lowest 1^+ states in ^{56}Fe and ^{82}Ge have energies 4.06 and 2.67 MeV, respectively. Note, that the experimental energy of the first 1^+ excited state in ^{56}Fe is 3.12 MeV.

For the ground-state cross-sections we also analyze the effect due to the exploitation of the full q-dependent 1^+ transition operator instead of its long wavelength limit. In the latter case the 1^+ operator reduces to the Gamow-Teller operator

$$\mathrm{GT}_0 = \left(\frac{g_A}{g_V}\right)\vec{\sigma}t_0, \quad (13)$$

where $(g_A/g_V) = -1.2599$ [38] is the ratio of the axial and vector weak coupling constants and t_0 denotes the zero component of the isospin operator in spherical coordinates. Here we would like to remind that within the hybrid approach [6, 8, 9], the GT contribution to the cross-section is obtained by using the large-scale shell-model calculations. Therefore, to make a comparison with the hybrid approach calculation more transparent, we use the same quenching factor for the axial weak coupling constant, $g_A^* = 0.74 g_A$, when calculating the matrix elements of the 1^+ transition operator.

Let us first demonstrate the calculated QRPA (quenched) GT$_0$ strength distributions. Referring to Fig. 2, at zero temperature the GT$_0$ strength is concentrated in the resonance state around $E = 10$ MeV. According to our QRPA calculations, the main contribution to the GT$_0$ resonance in ^{56}Fe comes from the proton and neutron single-particle transitions $1f_{7/2} \rightarrow 1f_{5/2}$. In

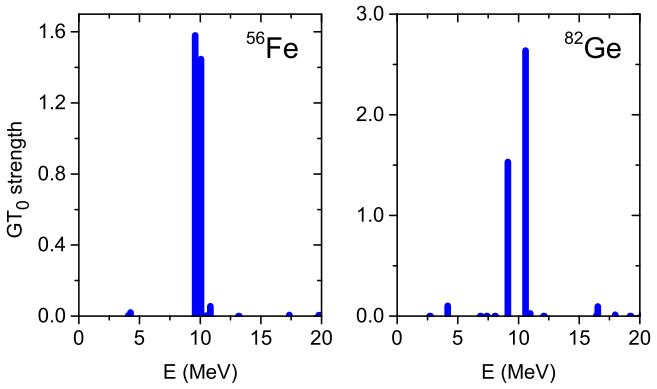

FIG. 2. (Color online) The distributions of the GT_0 strength in ^{56}Fe and ^{82}Ge.

^{82}Ge, the neutron transition $1g_{9/2} \to 1g_{7/2}$ also contributes to the resonance. In addition, for both nuclei our QRPA calculations predict a weak low-lying GT_0 strength ($E \approx 4$ MeV) arising from the $2p_{3/2} \to 2p_{1/2}$ single-particle transitions. For ^{56}Fe, the gross-structure of the GT_0 strength distribution agrees quite well with the shell-model results [9], meaning that the GT_0 strength is concentrated in the resonance region around 10 MeV with a small bump at low energy. The same good agreement can be found if we compare the shell-model GT_0 distributions for ^{54}Fe (see Ref. [9]) with our previously reported QRPA result [13]. However, although our calculations reproduce the resonance positions in ^{54,56}Fe, it is a well-known fact that the QRPA fails to recover all nuclear correlations needed to correctly describe the full resonance width and produces only a part of it, the so-called Landau width. The latter is quite small for the GT_0 resonance. As a result, the fine structure of GT distributions in the vicinity of the resonance is not reproduced in our calculations. In this respect the shell-model calculations are clearly advantageous.

Using the calculated strength distributions we apply Eq. (11) and calculate the GT contribution to the ground-state cross-sections. In Fig. 1, these contributions are shown by the dash-double dotted lines. From the figure we conclude that for neutrino energies $E_\nu < 20$ MeV, when 1^+ transitions dominate the cross-section, application of the GT_0 operator instead of the q-dependent 1^+ operator is fully justified. However, for neutrinos with the energy 30 MeV $< E_\nu <$ 60 MeV the GT_0 operator overestimates the cross-sections by about 25%.

In Table I, we compare the calculated ground-state cross-sections for ^{56}Fe with those obtained with the hybrid approach [8], the relativistic self-consistent QRPA [26], and the QRPA-based framework from Ref. [39]. The range of incoming neutrino energies is $10 \le E_\nu \le 100$ MeV. As it follows from the table, except for low neutrino energies ($E_\nu = 10$ MeV), the cross-sections of all four models are in good qualitative agreement. It is interesting to note that for $E_\nu \ge 20$ MeV the present results are generally closer to the hybrid approach results than the results of the other two QRPA-based methods.

TABLE I. The cross-sections (in units of 10^{-42} cm^2) for inelastic neutrino scattering on the ground state of ^{56}Fe. The present QRPA results (second column) are compared with those from [26, 39] and with the hybrid approach results [8].

E_ν (MeV)	QRPA	QRPA[26]	QRPA[39]	Hybrid[8]
10	1.69(-2)	1.87(-1)	1.01(+0)	1.91(-1)
20	5.64(+0)	9.78(+0)	5.79(+0)	6.90(+0)
30	2.41(+1)	4.08(+0)	1.87(+1)	2.85(+1)
40	6.65(+1)	1.05(+2)	5.51(+1)	7.86(+1)
50	1.49(+2)	2.16(+2)	1.43(+2)	1.72(+2)
60	2.87(+2)	3.89(+2)	3.09(+2)	3.20(+2)
70	4.83(+2)	6.33(+2)	5.63(+2)	5.25(+2)
80	7.36(+2)	9.59(+2)	8.82(+2)	7.89(+2)
90	1.03(+3)	1.38(+3)	1.22(+3)	1.11(+3)
100	1.36(+3)	1.92(+3)	1.52(+3)	1.49(+3)

To explain the discrepancy between our calculations and those of the hybrid approach at low neutrino energies, we note that at $E_\nu \approx 10$ MeV the calculated cross-sections are strongly sensitive to the fine details of the GT_0 distribution in the resonance region. As it was already discussed above, the large-scale shell-model calculations adequately reproduce the fragmentation of the GT_0 resonance strength whereas the QRPA calculations predict its much stronger concentration near the excitation energy $E \approx 10$ MeV. For this reason, our cross-section calculated for $E_\nu = 10$ MeV is considerably smaller than the hybrid approach result.

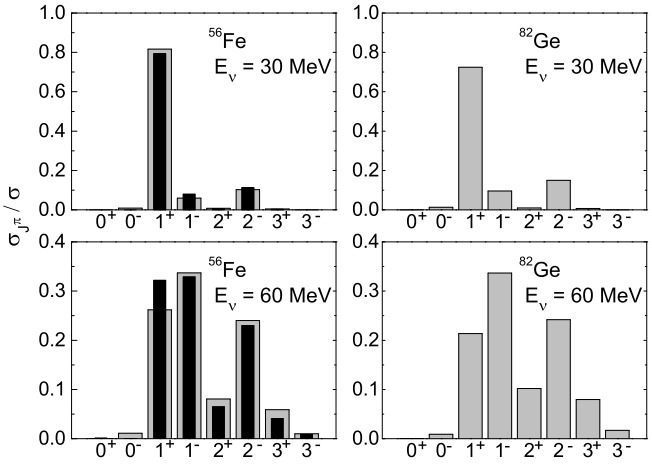

FIG. 3. Relative contributions of multipole transitions $J^\pi = 0^\pm - 3^\pm$ in the cross-sections for the inelastic neutrino scattering on the ground-states of ^{56}Fe and ^{82}Ge at incoming neutrino energies $E_\nu = 30$ and 60 MeV. For ^{56}Fe, the results of the present analysis (grey bars) are compared with the results of relativistic self-consistent QRPA calculations (black bars). The latter are obtained from Fig. 3 in Ref. [26].

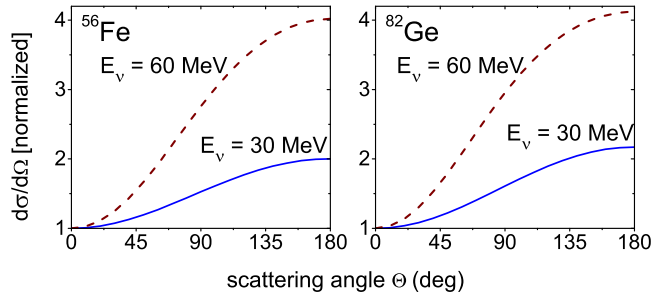

FIG. 4. (Color online) Normalized differential cross-sections as a function of the scattering angle.

We also study how relative contributions of different multipoles to the total cross-sections depend on the energy of incoming neutrinos. In Fig. 3, the relative contributions are shown for $E_\nu = 30$ and 60 MeV neutrinos. Even at $E_\nu = 30$ MeV a largely dominant multipole is 1^+, although contributions coming from the other multipoles are not negligible. For ^{82}Ge this contribution reaches about 30% of the total cross-section. This is due to the neutron excess which makes possible spin-dipole 1^- and 2^- $1\hbar\omega$ transition at relatively low neutrino energies. The situation is quite different for $E_\nu = 60$ MeV where the multipole transitions $J^\pi = 1^+$, 1^- and 2^- contribute about equally to the cross-sections.

In Fig. 3, we compare the obtained multipole composition of the cross-section for ^{56}Fe with that from relativistic self-consistent QRPA calculations [26]. Although our cross-sections are somewhat smaller than those in Ref. [26] (compare the second and the third columns of Table I), one can observe an excellent agreement between the two models based on rather different backgrounds. In accordance with Ref. [26], we find that 0^+ allowed transitions only marginally contribute to the inelastic cross-section and this finding is true for finite temperatures as well. For this reason, in the discussion below, we will always mean only the 1^+ multipole channel when considering the allowed transitions.

The angular distributions of the scattered neutrinos are shown in Fig. 4 for two incoming neutrino energies, $E_\nu = 30$ and 60 MeV. To make the presentation more transparent, we normalize the calculated differential cross sections to their value at $\Theta = 0°$. As shown in the figure, neutrinos scatter predominately in the backward direction. For $E_\nu = 30$ MeV, when 1^+ transitions dominate, the momentum transfer is small and the angular dependence of the differential cross-section essentially corresponds to $d\sigma/d\Omega \sim (1 + \sin^2(\Theta/2))$ [24]. The small deviation for ^{82}Ge is due to a non-negligible contribution from the forbidden multipoles (see Fig. 3). For $E_\nu = 60$ MeV neutrinos, owing to the dominant contribution of forbidden multipoles, the backward-to-forward asymmetry of the differential cross-sections becomes more pronounced.

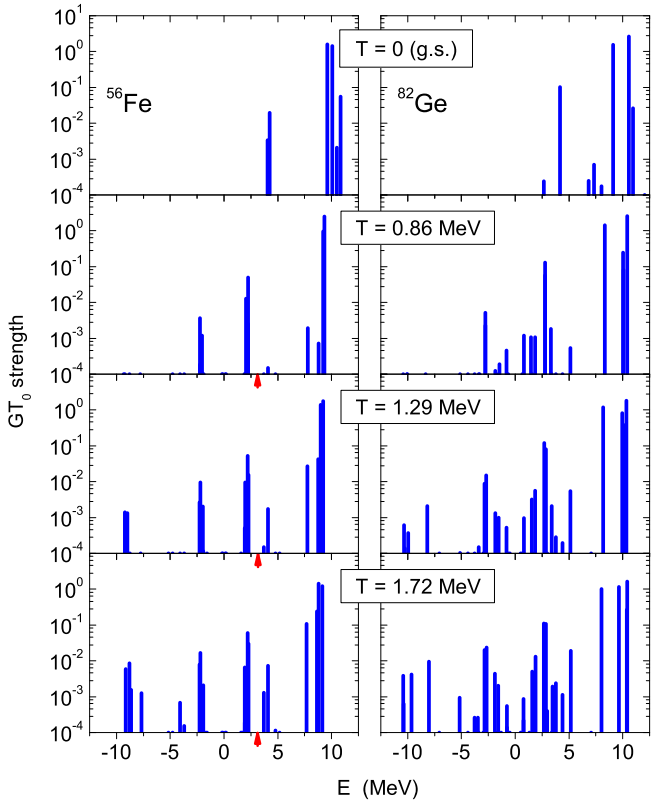

FIG. 5. (Color online) Temperature evolution of GT_0 strength distributions for ^{56}Fe (left panels) and for ^{82}Ge (right panels) vs. transition energy. The latter is equivalent to the neutrino energy transfer. The arrows indicate the zero-temperature threshold $E_{\rm exp}(1_1^+) = 3.12$ MeV for inelastic neutrino scattering off ^{56}Fe.

B. Finite temperatures

Now we turn our discussion to thermal effects on the inelastic neutrino-nucleus scattering. We start by considering the temperature evolution of the strength distributions for GT_0 transitions which dominate low-energy neutrino scattering. In Fig. 5, we display on a logarithmic scale the GT_0 strength distributions at three different temperatures relevant in the supernova context [6]: $T = 0.86$ MeV corresponds to the condition in the core of a presupernova model for a $15M_\odot$ star; $T = 1.29$ MeV and $T = 1.72$ MeV relate approximately to neutrino trapping and neutrino thermalization stages, respectively. The transition energy E refers to the excitation energy of a thermal one-phonon state and is equivalent to the neutrino energy transfer. To make the thermal effects more visible, the ground-state GT_0 distributions are displayed in Fig. 5 as well.

Since the Brink hypothesis is not valid within our approach, in Fig. 5 we observe a redistribution of the GT_0 strength for upward transitions ($E > 0$). Namely, at temperatures above the critical one no extra energy has be paid to break a Cooper pair. Therefore, by virtue of the

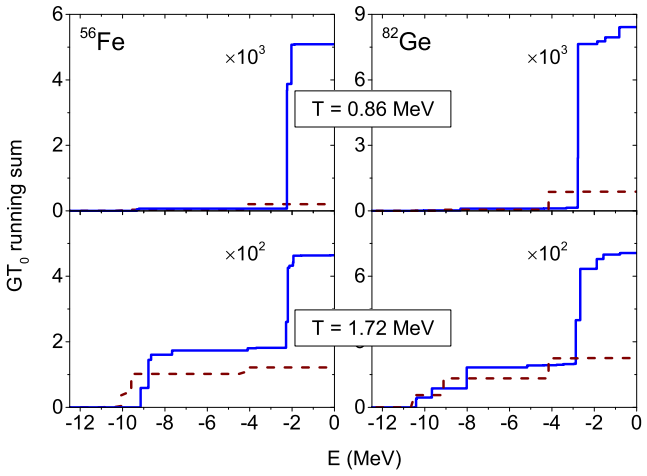

FIG. 6. (Color online) Comparison of the running sums for GT_0 downward strength distributions obtained using (dashed lines) and without using (solid lines) the Brink hypothesis. Note, that the values are scaled by a factor of 10^3 ($T = 0.86\,\mathrm{MeV}$) and 10^2 ($T = 1.72\,\mathrm{MeV}$).

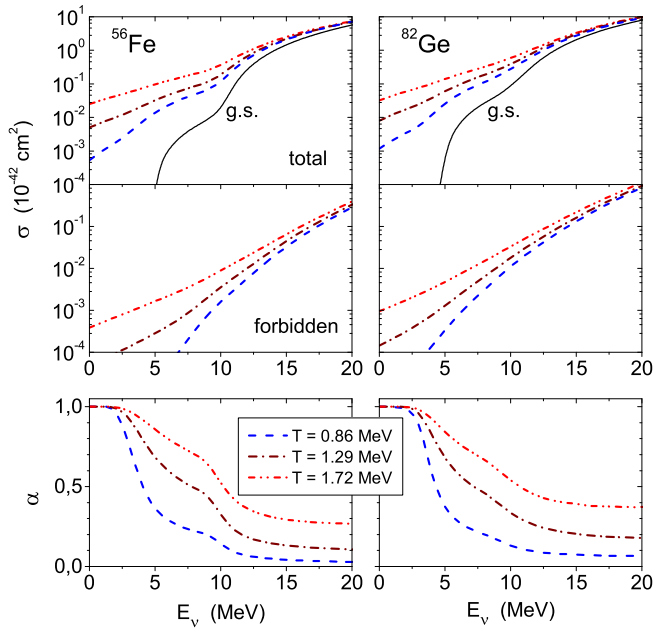

FIG. 7. (Color online) Upper panels: Total inelastic neutrino scattering cross sections for ^{56}Fe and ^{82}Ge at three different temperatures relevant for core-collapse. For comparison the ground-state cross-sections are also shown. Middle panels: Contributions of forbidden transitions to the finite-temperature cross-sections. Lower panels: Temperature dependence of the fraction of down-scattered neutrinos in the thermal enhancement of the cross-section.

vanishing of pairing correlations, both the GT_0 resonance and its low-energy tail move to lower energies. Our calculations indicate that, with increasing temperature up to 1.72 MeV, the resulting resonance energy shift reaches about 1.5 MeV in ^{56}Fe and 1.2 MeV in ^{82}Ge. It is interesting to note that within the present TQRPA calculations for ^{56}Fe the low-lying GT_0 strength shifts below the zero-temperature threshold (i.e., below the experimental energy of the first 1^+ state). Furthermore, the thermal smearing of the nuclear Fermi surface makes low-energy particle-particle and hole-hole transitions possible which are Pauli-blocked at zero temperature. Such thermally-unblocked transitions enhance the low-lying component of the GT_0 distributions and make it more fragmented. Since the ^{82}Ge nucleus has a larger single-particle level density near the Fermi surface, the temperature-induced enhancement and fragmentation of the low-lying GT_0 upward strength is more significant than in ^{56}Fe.

Here we would like to stress that the appearance of a sizeable amount of the low-lying transition strength in nuclei at $T \neq 0$ is predicted in all theoretical studies of hot nuclei. For example, this was found already in one of the first papers on the subject Ref. [40], where the distributions of the electric $E1$ and $E3$ transitions at $T \neq 0$ in ^{208}Pb were calculated and in many subsequent studies (see, e.g., [10, 11, 41]. The same effect is predicted for the charge-exchange allowed and first-forbidden transitions as well [17, 27]. For the charge-exchange Gamow-Teller transitions this feature was also obtained within the shell-model Monte-Carlo theory [12]. Moreover, shell-model Monte-Carlo calculations demonstrate that with increasing temperature the centroid of the GT_+ resonance shifts to lower energies.

Focusing our attention on the negative energy downward transitions we observe from Fig. 5 that the corresponding GT_0 strength increases with increasing temperature. This is just a consequence of detailed balance (6): the higher the temperature, the more substantial is the population of nuclear excited states and hence, the higher is the probability to gain energy from a hot nucleus. Note that the GT_0 strength around $E_\nu \approx -9\,\mathrm{MeV}$ can be attributed to the deexcitation of the GT_0 resonance. Given the importance of thermal effects on the upward strength distributions, it is worthwhile to examine how the violation of Brink's hypothesis affects the downward strength. It is obvious that the shift of the GT_0 distributions to lower energies and the appearance of low-energy transitions should magnify the strength of downward transitions. This effect is clearly demonstrated in Fig. 6 which shows running sums for the GT_0 downward strength distributions derived by using the Brink hypothesis or not. The former are obtained from the ground-state ($T = 0$) distributions by multiplication with the Boltzmann factor $\exp(-E/T)$. Referring to the figure, the considerable increase of the overall downward strength is mainly caused by the thermal effects on the low-energy tail in the GT_0 distributions. This is most pronounced at low temperatures ($T = 0.86\,\mathrm{MeV}$). However, at high temperatures ($T = 1.72\,\mathrm{MeV}$) the GT_0 resonance becomes thermally populated and its shift to lower energies also contributes to the downward strength increase.

The detailed discussion above allows us to under-

stand better the thermal effects on the inelastic neutrino-nucleus scattering. In the top panels of Fig. 7, we compare the ground-state cross-sections with those calculated at the three core-collapse temperatures. As follows from our calculations, temperature effects are unimportant for $E_\nu > 20$ MeV when neutrinos have sufficiently large energy to excite the GT_0 resonance and collective excitations with other multipolarities. Note that a downward shift of the GT_0 resonance only marginally affects the cross-sections at such high neutrino energies. However, as one can see from the plots, the cross-sections significantly depend on temperature for low-energy neutrinos. Namely, the reaction threshold disappears and the cross-sections are enhanced by up to two orders of magnitude when the temperature rises from 0.86 MeV to 1.72 MeV. It is significant that all these features have pointed out in [5, 6, 13] as well.

In Fig. 7, we also demonstrate the overall contribution of the forbidden transitions $J^\pi = 0^-$, 1^-, $2^\pm$, $3^\pm$ to the cross-sections. In contrast to hybrid approach calculations [6] their contributions are temperature dependent. However, comparing the upper and middle panels of Fig. 7, one concludes that the enhancement of the cross-sections at finite temperatures is essentially due to thermal effects on the GT_0 transition strengths.

At vanishing neutrino energies, $E_\nu \approx 0$, the finite temperature cross-sections are given by the second, up-scattering, term in Eq. (11) which accounts for the GT_0 downward transitions from thermally excited nuclear states. As shown in Fig. 5 and pointed out previously, the strength of such transitions increases with temperature thereby enhancing the cross-sections. However, in our approach due to the violation of the Brink hypothesis, the down-scattering part of the cross-section, $\sigma_{\rm down}$, is also temperature dependent and it increases with temperature owing to the thermally unblocked low-energy GT_0 transitions and the downward shift of the GT_0 resonance. This effect is clearly shown in Ref. [13] for ^{54}Fe.

To analyze relative importance of the two types of neutrino scattering processes in the thermal enhancement of the cross-section, we introduce the ratio α

$$\alpha = \frac{\sigma_{\rm up}(T)}{\sigma(T) - \sigma_{\rm g.s.}}, \qquad (14)$$

where the difference $\sigma(T) - \sigma_{\rm g.s.}$ represents an overall enhancement of the cross-section due to thermal effects. Note that within the hybrid approach $\alpha = 1$, because $\sigma(T) = \sigma_{\rm g.s.} + \sigma_{\rm up}(T)$ in this approach. We plot the ratio α in the lower panels of Fig. 7 as a function of E_ν for the selected temperatures. As expected, the ratio $\alpha \sim 1$ for low-energy neutrinos and then, with increase of E_ν, α gradually decreases indicating a rising contribution of the up-scattering process to the cross-section thermal enhancement. It is seen from the plots that for 5 MeV $< E_\nu <$ 10 MeV neutrinos, both from the up-scattering and down-scattering processes contribute to the noticeable enhancement of the cross-sections, although their relative importance depends on temperature: the higher the temperature the more important is the contribution of the up-scattering process. Consequently, even for $E_\nu \approx 10$ MeV neutrinos, when the excitation of the GT_0 resonance becomes possible, the up-scattering component of the cross-section appears to be comparable with the down-scattering one for temperatures $T \geq 1.29$ MeV.

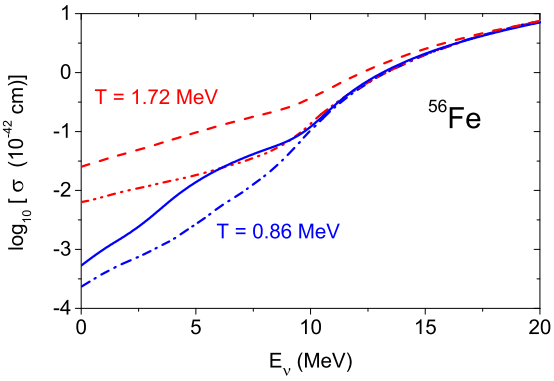

FIG. 8. (Color online) Comparison of the cross-sections of neutrino inelastic scattering off the hot nucleus ^{56}Fe calculated within the present TQRPA approach and the hybrid approach (Ref. [6], Fig. 11). The solid and dashed lines show the present results for $T = 0.86$ MeV and $T = 1.72$ MeV, respectively. The dash-dotted and dash-double-dotted lines show results from Ref. [6] for the same T values.

In Fig. 8, we compare our results for ^{56}Fe with those obtained within the hybrid approach [6]. The comparison is made for temperatures $T = 0.86$ and 1.72 MeV. As one can see, at $E_\nu < 10$ MeV there is noticeable disagreement between the results of the two approaches: The TQRPA cross-sections are larger by a factor of 2 to 5 than the hybrid approach ones. To understand the cause of the discrepancy, we calculate the spectrum of outgoing neutrinos scattered off ^{56}Fe at the same temperatures as in Fig. 8 and compare the results with the hybrid approach calculations (see Fig. 13 of Ref. [6]). In Fig. 9, the spectra are shown for the same initial neutrino energies as in Ref. [6]: $E_\nu = 5$, 10, and 15 MeV. Note that for a clearer presentation and for comparison convenience, the TQRPA spectra are normalized to unity and folded with the Breit-Wigner function with a width of 1 MeV.

At low temperatures, the downward transitions from the thermally excited GT_0 resonance are strongly suppressed by the Boltzmann factor. Therefore, for $T = 0.86$ MeV and $E_\nu = 5$ MeV the spectrum is dominated by neutrinos up- and down-scattered due to the low-energy GT_0 transitions. In Fig. 9, such transitions correspond to the sizable peaks in the spectrum at around $E_{\nu'} \sim (E_\nu \pm 2.5\,{\rm MeV})$. The dominance of low-energy up- and down-transitions in the scattering of low-energy neutrinos off ^{56}Fe at $T = 0.86$ MeV is also supported by the hybrid approach studies (see the upper-middle panel of Fig. 13 in Ref. [6]). However, the energy and the strength of such transitions calculated with the TQRPA

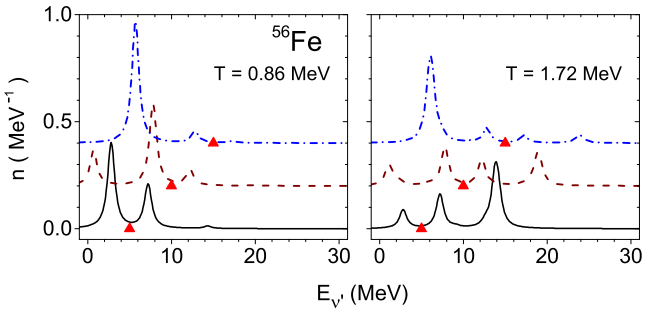

FIG. 9. (Color online) Normalized spectra of outgoing neutrinos for ^{56}Fe at $T = 0.86$ MeV and 1.72 MeV and three initial neutrino energies: $E_\nu = 5$ MeV (solid line), 10 MeV (dashed line, all values shifted by 0.2), and 15 MeV (dash-dotted line, all values shifted by 0.4). The triangles correspond to the energy of the incoming neutrino.

and the hybrid approach are different. As discussed in detail above, within the TQRPA thermal effects shift the low-lying GT strength in ^{56}Fe to energies below the zero-temperature threshold (Fig. 5) and significantly increase the strength of the corresponding inverse downward transitions (Fig. 6), thus favoring neutrino inelastic scattering. No such effects are expected within the hybrid approach due to the application of the Brink hypothesis. For this reason, the low-energy ($E_\nu < 10$ MeV) TQRPA cross-section at $T = 0.86$ MeV appears to be larger than the hybrid approach one. With increasing energy of incoming neutrinos, the excitation of the GT_0 resonance comes into play as evidenced by peaks in the spectra around $E_{\nu'} \sim (E_\nu - 9\,\text{MeV})$. Consequently, the cross-section becomes less sensitive to thermal effects on the low-lying GT_0 strength. As a consequence for $E_\nu > 10$ MeV we observe excellent agreement between the TQRPA and the hybrid approach results.

The situation is slightly different for the higher temperature, $T = 1.72$ MeV. Now downward transitions from the thermally excited GT_0 resonance are possible, and owing to a large phase-space factor they can contribute significantly to the up-scattering of low-energy neutrinos. In the spectra this contribution corresponds to the peak at around $E_{\nu'} \sim (E_\nu + 9\,\text{MeV})$. As indicated in Fig. 6, at $T = 1.72$ MeV thermal effects increase the strength of downward transitions from the GT_0 resonance. Although this increase is not of the same magnitude as for the low-lying GT_0 strength, due to a larger phase-space factor, its contribution to the cross-section enhancement is substantial. Therefore, one can conclude that at $T = 1.72$ MeV the joint action of thermal changes in both the low-lying GT_0 strength and the GT_0 resonance enhances the absolute value of the TQRPA cross-section at $E_\nu \lesssim 10$ MeV in comparison with the hybrid approach. Like for the $T = 0.86$ MeV case, thermal effects become less important for higher neutrino energies, and both approaches yield very similar results for the cross-sections.

Considering thermal effects on angular distributions of outgoing neutrinos we find that they are rather unimportant. For up-scattered neutrinos these distributions are only slightly more backward peaked than those for down-scattered neutrinos owing to the larger momentum transfer.

IV. CONCLUSION

We have studied thermal effects on the inelastic neutrino-nucleus scattering in the supernova environment. The thermal effects were treated within the thermal quasiparticle random phase approximation. The calculations were performed for ^{56}Fe and ^{82}Ge.

We find that the TQRPA calculations do not support the Brink hypothesis and lead to temperature-dependent strength distributions for both allowed and forbidden transitions involved in the neutrino inelastic scattering. It is shown that thermal effects shift the GT_0 centroid to lower energies and make low-energy GT_0 transitions possible. As a result, in contrast to hybrid approach calculations [6], both the up-scattering and down-scattering components of the cross-section exhibit a noticeable temperature dependence at low-energy neutrinos.

Our calculations reveal the same thermal effects as the hybrid approach based calculations. Namely, the reaction threshold for inelastic neutrino-nucleus scattering is removed at finite temperatures and the cross-section for low-energy neutrinos is significantly enhanced.

However, the calculated cross-sections for ^{56}Fe at low neutrino energies are several times larger than those obtained within the hybrid approach. We have shown that the discrepancy is due to the violation of Brink's hypothesis in our approach. This is the main result of the present study. In addition, it has been demonstrated that the TQRPA approach can be used to study inelastic neutrino scattering off massive neutron-rich nuclei at finite temperatures. Another advantage of our approach is that it incorporates the detailed balance principle, whereas in the hybrid approach detailed balance is violated.

There are several directions to improve our approach. At present, its predictive power is limited by the phenomenological Hamiltonian with schematic separable residual interactions. It would therefore be desirable to combine our TFD-based TQRPA method with self-consistent QRPA calculations based on more realistic effective interactions. For neutrino scattering and neutrino absorption reactions at zero temperature, such calculations were performed recently within the relativistic nuclear density functional theory [26, 42]. This improvement would also allow to take into account the effects of nuclear deformation. For supernova electron-capture rates in pf-shell nuclei, deformation was recently included in self-consistent QRPA calculations with the Skyrme interaction [43]. The other direction of improvement is the inclusion of correlations beyond the TQRPA by taking into account the coupling of thermal phonons with more complex (e.g. two-phonon) configurations. At

zero temperature this problem was considered within the QPM [28] by exploiting separable schematic effective interactions. However, with the separable approximation for the Skyrme interaction [44] one could consider phonon coupling at finite temperatures within a self-consistent theory.

ACKNOWLEDGMENTS

The collaboration with Prof. T. S. Kosmas and Dr. V. Tsakstara from the University of Ioannina is acknowledged. We are also greatly indebted to Prof. G. Martínez-Pinedo for helpful discussions and important comments on this paper. This work was supported in part by the Heisenberg-Landau Program, the CNRS-RFBR grant 11-091054, and the Deutsche Forschungsgemeinschaft grant No. SFB 634.

[1] H.-T. Janka, K. Langanke, A. Marek, G. Martínez-Pinedo, and B. Müller, Physics Reports **442**, 38 (2007), the Hans Bethe Centennial Volume 1906-2006.
[2] W. C. Haxton, Phys. Rev. Lett. **60**, 1999 (1988).
[3] S. W. Bruenn and W. C. Haxton, Astrophys. J. **376**, 678 (1991).
[4] K. Langanke, G. Martínez-Pinedo, B. Müller, H.-T. Janka, A. Marek, W. R. Hix, A. Juodagalvis, and J. M. Sampaio, Phys. Rev. Lett. **100**, 011101 (2008).
[5] G. M. Fuller and B. S. Meyer, Astrophys. J. **376**, 701 (1991).
[6] A. Juodagalvis, K. Langanke, G. Martínez-Pinedo, W. Hix, D. Dean, and J. Sampaio, Nuclear Physics A **747**, 87 (2005).
[7] J. Sampaio, K. Langanke, G. Martínez-Pinedo, and D. Dean, Physics Letters B **529**, 19 (2002).
[8] E. Kolbe and K. Langanke, Phys. Rev. C **63**, 025802 (2001).
[9] J. Toivanen, E. Kolbe, K. Langanke, G. Martínez-Pinedo, and P. Vogel, Nuclear Physics A **694**, 395 (2001).
[10] P. Bortignon, A. Bracco, and R. Broglia, *Giant Resonances: Nuclear Structure at Finite Temperature*, Contemporary concepts in physics (Harwood Academic Publishers, 1998).
[11] D. Santonocito and Y. Blumenfeld, The European Physical Journal A - Hadrons and Nuclei **30**, 183 (2006).
[12] P. B. Radha, D. J. Dean, S. E. Koonin, K. Langanke, and P. Vogel, Phys. Rev. C **56**, 3079 (1997).
[13] A. Dzhioev, A. Vdovin, V. Ponomarev, and J. Wambach, Physics of Atomic Nuclei **74**, 1162 (2011).
[14] Y. TakahashI and H. Umezawa, International Journal of Modern Physics B **10**, 1755 (1996).
[15] H. Umezawa, H. Matsumoto, and M. Tachiki, *Thermo field dynamics and condensed states* (North-Holland Pub. Co., 1982).
[16] I. Ojima, Annals of Physics **137**, 1 (1981).
[17] A. A. Dzhioev, A. I. Vdovin, V. Y. Ponomarev, J. Wambach, K. Langanke, and G. Martínez-Pinedo, Phys. Rev. C **81**, 015804 (2010).
[18] A. A. Dzhioev and A. I. Vdovin, International Journal of Modern Physics E **18**, 1535 (2009).
[19] The correspondence between the thermo field dynamics and the superoperator formalism is discussed in [45]. The latter is used by one of the authors (A.D.) to study nonequilibrium transport phenomena (see, e.g., [46]).
[20] R. Kubo, Journal of the Physical Society of Japan **12**, 570 (1957); P. C. Martin and J. Schwinger, Phys. Rev. **115**, 1342 (1959).
[21] In Eq. (3), $[]^J_M$ denotes the coupling of two single-particle angular momenta j_1, j_2 to the total angular momentum J. The bar over index j means time-inversion.
[22] T. Fischer, K. Langanke, and G. Martínez-Pinedo, e-print arXiv:astro-ph.HE/1309.4271v1 (2013).
[23] J. D. Walecka, in *Muon Physics V2: Weak Interactions*, edited by V. W. Hughes and C. S. Wu (Elsevier Science, 1975) p. 113.
[24] T. W. Donnelly and R. D. Peccei, Physics Reports **50**, 1 (1979).
[25] S. Singh, Nuclear Physics B - Proceedings Supplements **112**, 77 (200
[26] H. Đapo and N. Paar, Phys. Rev. C **86**, 035804 (2012).
[27] J. Cooperstein and J. Wambach, Nuclear Physics A **420**, 591 (1984).
[28] V. G. Soloviev, *Theory of atomic nuclei: quasiparticles and phonons* (Taylor & Francis, 1992).
[29] V. A. Chepurnov, Yad. Phys. **6**, 955 (1967), [Sov. J. Nucl. Phys. **6**, 696 (1968)].
[30] A. L. Goodman, Nuclear Physics A **352**, 30 (1981).
[31] O. Civitarese, G. Dussel, and R. P. J. Perazzo, Nuclear Physics A **404**, 15 (1983).
[32] A. A. Dzhioev, A. I. Vdovin, V. Tsakstara, and T. S. Kosmas, Journal of Physics: Conference Series **410**, 012172 (2013).
[33] B. Castel and I. Hamamoto, Physics Letters B **65**, 27 (1976).
[34] D. R. Bes, R. A. Broglia, and B. Nilsson, Physics Reports **16**, 1 (1975).
[35] J. Rapaport, T. Taddeucci, T. Welch, C. Gaarde, J. Larsen, D. Horen, E. Sugarbaker, P. Koncz, C. Foster, C. Goodman, C. Goulding, and T. Masterson, Nuclear Physics A **410**, 371 (1983).
[36] R. T., H. Condé, N. Olsson, E. Ramström, R. Zorro, J. Blomgren, A. Håkansson, A. Ringbom, G. Tibell, O. Jonsson, L. Nilsson, P.-U. Renberg, S. Y. van der Werf, W. Unkelbach, and F. P. Brady, Nuclear Physics A **563**, 225 (1993).
[37] T. J. Bowles, R. J. Holt, H. E. Jackson, R. M. Laszewski, R. D. McKeown, A. M. Nathan, and J. R. Specht, Phys. Rev. C **24**, 1940 (1981).
[38] I. S. Towner, in *Symmetries and Fundamental Interactions in Nuclei*, edited by W. C. Haxton and E. M. Henley (World Scientific Publishing Company, Incorporated, 1995) p. 183.
[39] V. Chasioti, T. S. Kosmas, and P. Divari, Progress in Particle and Nuclear Physics **59**, 481 (2007).
[40] D. Vautherin and N. V. Mau, Nuclear Physics A **422**, 140 (1984).

[41] Y. F. Niu, N. Paar, D. Vretenar, and J. Meng, Physics Letters B **681**, 315 (2009).
[42] N. Paar, H. Tutman, T. Marketin, and T. Fischer, Phys. Rev. C **87**, 025801 (2013).
[43] P. Sarriguren, Phys. Rev. C **87**, 045801 (2013).
[44] N. Van Giai, C. Stoyanov, and V. V. Voronov, Phys. Rev. C **57**, 1204 (1998).
[45] M. Schmutz, Zeitschrift für Physik B Condensed Matter **30**, 97 (1978
[46] A. A. Dzhioev and D. S. Kosov, Journal of Physics: Condensed Matter **24**, 225304 (2012).